Dispersion of Magnetic Excitations in Optimally Doped Superconducting $YBa_2Cu_3O_{6.95}$

D. Reznik,[1,2,*] P. Bourges,[2] L. Pintschovius,[1] Y. Endoh,[3,4] Y. Sidis,[2] T. Masui,[5] and S. Tajima[5]
[1]*Forschungszentrum Karlsruhe, Institut für Festkörperphysik, Postfach 3640, D-76021 Karlsruhe, Germany*
[2]*Laboratoire Léon Brillouin, CEA-CNRS, CE-Saclay, 91191 Gif sur Yvette, France*
[3]*Institute for Material Research, Tohoku University, Katahira, Aoba-ku, Sendai, 980-8577, Japan*
[4]*International Institute for Advanced Studies, Kizugawadai, Kyoto, 619-0225, Japan*
[5]*Superconductivity Research Laboratory, ISTEC, Shinonome, Koutu-ku, Tokyo, 135-0062, Japan*
(Received 23 July 2003; published 10 November 2004)

Detailed neutron scattering measurements of $YBa_2Cu_3O_{6.95}$ found that the resonance peak and incommensurate magnetic scattering induced by superconductivity represent the same physical phenomenon: two dispersive branches that converge near 41 meV and the in-plane wave vector $\mathbf{q}_{AF} = (\pi/a, \pi/a)$ to form the resonance peak. One branch has a circular symmetry around $\mathbf{q}_{AF}$ and quadratic downward dispersion from ≈ 41 meV to the spin gap of 33 ± 1 meV. The other, of lower intensity, disperses from ≈ 41 meV to at least 55 meV. Our results exclude a quartet of vertical incommensurate rods in $\mathbf{q}$-ω space expected from spin waves produced by dynamical charge stripes as an origin of the observed incommensurate scattering in optimally doped YBCO.

DOI: 10.1103/PhysRevLett.93.207003 PACS numbers: 74.25.Ha, 74.72.Bk

The magnetic resonance peak observed by inelastic neutron scattering (INS) is one of the most striking features of high-T_c superconductors [1–7]. It corresponds to an unusual enhancement of spin fluctuations in the superconducting (SC) state at the planar antiferromagnetic (AF) wave vector $\mathbf{q}_{AF} = (\pi/a, \pi/a)$ at an energy E_r, which is found experimentally to scale with T_c as a function of hole doping. First discovered in optimally doped $YBa_2Cu_3O_{6+x}$ (YBCO) [1], its observation has then been extended to other systems such as $Tl_2Ba_2CuO_{6+x}$ [5] and $Bi_2Sr_2CaCu_2O_{8+x}$ [6]. The role of the magnetic resonance in measured changes of the fermionic properties of cuprates below T_c is hotly debated [8–10].

In underdoped $YBa_2Cu_3O_{6+x}$ ($x = 0.6$ [11], $x = 0.7$ [12,13], $x = 0.85$ [14]), INS measurements revealed additional incommensurate (IC) spin fluctuations at energies below E_r at low temperature. They may appear as reminiscent [11] of a quartet of peaks at planar wave vectors $\mathbf{q}_{ab} = (\pi/a(1 \pm \delta), \pi/a)$ and $(\pi/a, \pi/a(1 \pm \delta))$ observed in both the SC and the normal states of $La_{2-x}Sr_xCuO_4$ [15]. These are sometimes interpreted as spin waves originating from stripe fluctuations (fluctuating hole poor AF domains in antiphase separated by fluctuating lines of holes running along a^* or b^* [16]). However, in weakly underdoped $YBa_2Cu_3O_{6.85}$ [14], both energy and temperature dependencies of the incommensurability indicate that IC fluctuations and the magnetic resonance peak are part of a downward-dispersing magnetic collective mode that exists in the SC state only. Presently, the origin of the IC magnetic fluctuations, their interplay with the magnetic resonance peak, and their evolution with hole doping are still controversial issues.

The current study of $YBa_2Cu_3O_{6.95}$ focuses on the search for magnetic signatures of dynamical stripes and on the dispersion of the magnetic excitations at optimum doping. Throughout this Letter the wave vector $\mathbf{Q}$ (H, K, L) is indexed in reciprocal lattice units $(2\pi/a, 2\pi/b, 2\pi/c)$.

All INS experiments were performed on the 1T double focusing triple-axis spectrometer at the ORPHEE reactor. The 1.5 cm^3 sample with mosaic spread of 2.2° was made up of three coaligned high quality twinned single crystals of $YBa_2Cu_3O_{6+x}$ ($T_c = 93$ K). Lattice constants precisely measured by high resolution neutron diffraction were $a = 3.816$ Å, $b = 3.886$ Å, $c = 11.682$ Å. By comparison with Ref. [17], the unit cell volume as well as the a-b anisotropy indicate $x = 1$, the c-axis lattice constant gives $x = 0.92$, while the T_c is consistent with $x = 0.95$. A different very precise study of oxygen content versus lattice parameters in single crystals produced higher oxygen contents for the same c-axis lattice parameters [18], so we conclude that our sample had $x = 0.95 \pm 0.02$. The c axis was aligned close to vertical in order to access the

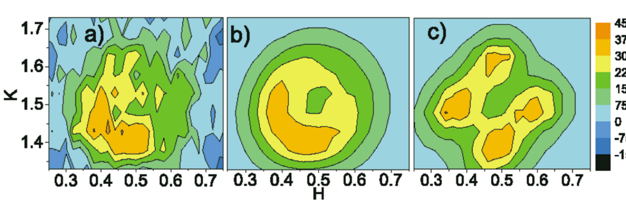

FIG. 1 (color). (a) A 10 K intensity minus 100 K intensity at 35 meV [same data as in Fig. 2(c)]. (b) Resolution-corrected model calculations [blue lines in Fig. 2(c)]. The lack of symmetry around $\mathbf{q}_{AF}$ is a focusing effect illustrated in Fig. 3(b), clearly indicating dispersion. (c) Resolution-corrected stripe model predictions. The small differences in intensities of the four spots are due to the magnetic form factor. Magnetic correlation length used here was the same as in (b) (see text).

 0031-9007/04/93(20)/207003(4)$22.50

entire Brillouin zone adjacent to $\mathbf{Q} = (3/2, 1/2, 1.7)$. Relaxed vertical resolution in this orientation maximizes magnetic intensity, which is broad in the c direction. The tilt of the sample changed during the scans to achieve the desired component of $\mathbf{q}$ perpendicular to the ab plane (q_c). A pyrolytic graphite (PG) filter minimized contamination from higher order neutrons. A PG002 monochromator and analyzer fixed at the final energy of 14.8 meV was chosen for the study at 35 meV [Figs. 1(a) and 2(c)]. For the scans between 35 and 55 meV [Fig. 2(a)] we used a Cu111 monochromator and PG002 analyzer fixed at 30.5 meV. We also found an experimental condition that dramatically improved spectrometer resolution over all previous measurements (energy resolution of ≈ 2.2 meV FWHM; the longitudinal and transverse q resolutions of ≈ 0.11 and ≈ 0.2 Å^{-1}, respectively), and allowed looking at the resonance peak in a "magnifying glass" [Fig. 2(b)]. Here we used a Cu220 monochromator and a PG002 analyzer fixed at 15.2 meV. At energies far above the resonance peak only a limited part of $\mathbf{q}$ space was measured because the kinematics of the neutron allow access to only a small part of the Brillouin zone. Using an unpolarized neutron beam, we relied on the standard technique of using temperature dependence to distinguish magnetic and nuclear scattering [3,4].

Constant energy scans at $E = 41$ meV and $T = 100$ K showed only a flat background agreeing with previous results for this composition [3,4]. However, rather strong

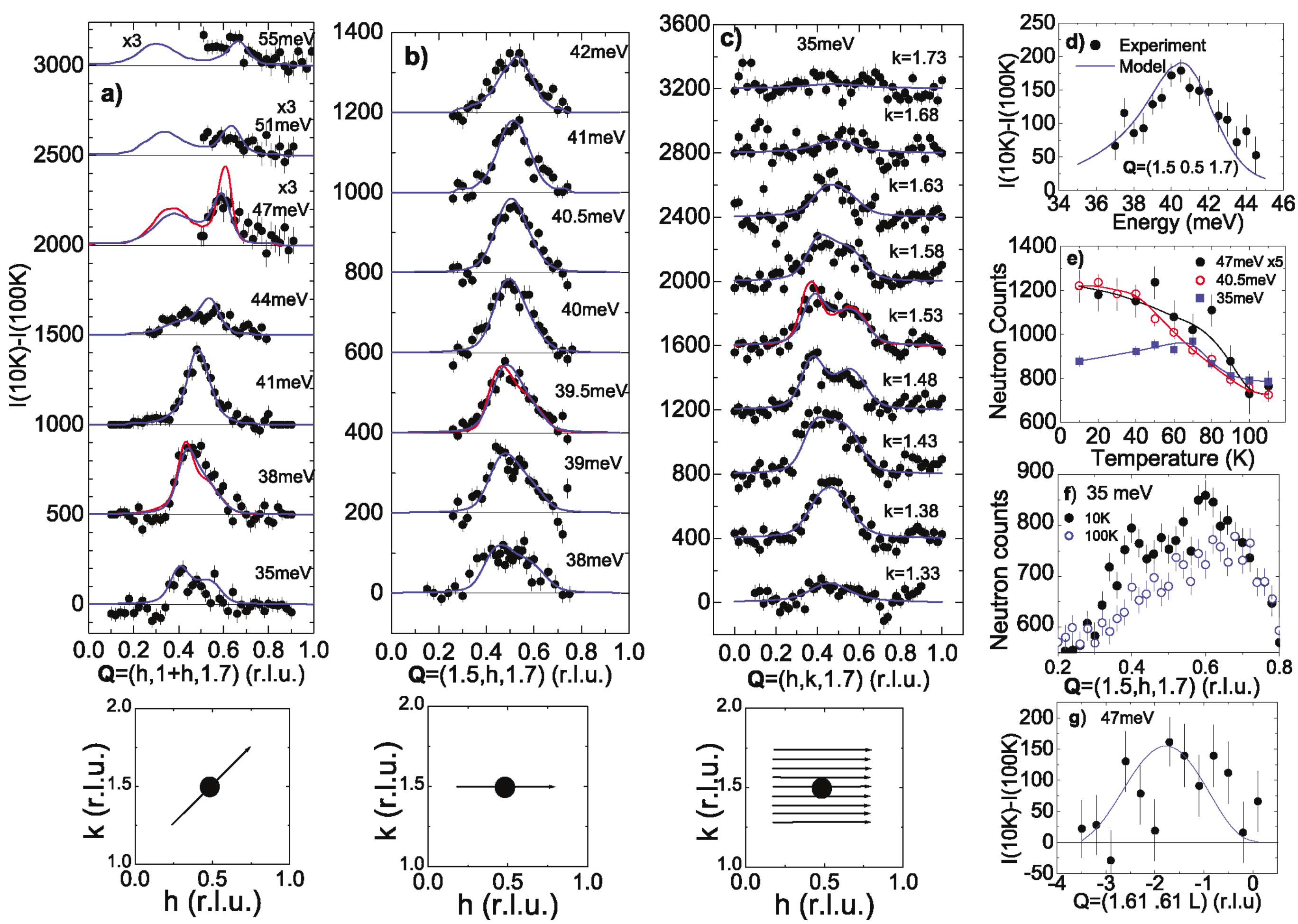

FIG. 2 (color). (a)–(d) Intensity at 10 K minus intensity at 100 K (data points) compared with the model illustrated in Fig. 3 convoluted with the resolution function. Blue and red lines represent, respectively, the model with and without the broadening described in the text. The energy resolution was (a) 5 meV, (b) and (d) 2.2 meV, and (c) 4 meV. A small linear term was subtracted from the scans in (c) to make the background the same on both sides. Overall amplitude differs for (a), (b), and (d), and (c), but is the same for each set of calculated curves. The diagrams below (a), (b), and (c) represent the scan directions projected onto the h-k plane for the plots above. (e) Scattering intensity at $(\mathbf{Q}, \omega) = ((1.4\ 0.4\ 1.7), 35\ \text{meV})$, $((1.5\ 0.5\ 1.7), 40.5\ \text{meV})$, and $((1.6\ 0.6\ 1.7), 47\ \text{meV})$ vs temperature. Constant intensity was subtracted from 35 and 47 meV data to scale together the 10–100 K intensities. (f) High resolution scans at 35 meV measured with Cu220/PG002 monochromator/analyzer and $E_f = 30.5$ meV at 100 and 10 K. (g) Intensity at 10 K minus intensity at 100 K (data points) compared with the odd bilayer magnetic structure factor (blue line).

features with **q** dependence expected from magnetic scattering persisted to 100 K at $E = 44$ meV and above. Further heating to 300 K did not make them disappear entirely. Therefore, their magnetic origin needs to be confirmed by further measurements. In the following, our analysis is based on intensity differences between 10 and 100 K, which are confidently assigned to magnetic scattering.

In order to search for evidence of dynamical stripes in optimally doped YBCO we mapped in **Q** space the scattering intensity at 35 meV, which is just above the measured spin gap of 33 ± 0.5 meV (data not shown in figures) and well below E_r ($\approx$41 meV). High resolution scans at 10 and 100 K in Fig. 2(f) clearly show the extra IC magnetic scattering appearing at 10 K on top of a broad feature originating from phonons. The contour plot of the intensity difference between 10 and 100 K at 35 meV [Fig. 1(a)] measured with a lower resolution also clearly shows an IC magnetic signal. The strong asymmetry around $\mathbf{q}_{\rm AF}$, a high symmetry point of the YBCO reciprocal lattice, can be easily explained by the tilt of the resolution ellipsoid in **q**-ω space that breaks the symmetry in the experiment and results in well understood focusing or defocusing effects. We find that a spectral function $S(\mathbf{q}, \omega)$ that is dispersive and circularly symmetric around $\mathbf{q}_{\rm AF}$ closely matches the data [Figs. 1(b) and 2(c)]. The observed intensity distribution contrasts with the quartet of peaks emerging from each incommensurate wave vector usually expected in the spin wave model of a stripe picture, which describes very well the magnetic response of the stripes in the nickelates [19]. In our case the "spin waves due to stripes" model differs from the data far beyond the experimental uncertainty even for a finite stripe correlation length [Fig. 1(c)]. However stripelike correlations can still be present if their excitation spectrum differs from spin waves as seems to be the case in $La_{1.875}Ba_{0.125}CuO_4$ [20].

Further measurements [Fig. 2(a)] revealed that the magnetic signal at 35 meV arises from a branch that disperses to lower energies from E_r and cuts off at the spin gap. We also found another branch that disperses upward above E_r persisting above 55 meV. This upper branch has not been previously observed because its peak intensity at energies where it is well separated from the lower branch is much smaller than at E_r. The raw data at 47 meV and 10 K (not shown in figures) were consistent with circular symmetry and not with four IC peaks, though they do not rule out a more complex **q**-space line shape. Figure 2(e) shows temperature dependence at three energies with **q** fixed at the maximum of the intensity change between 10 and 100 K at each energy. The intensities at 40.5 and 47 meV increase and then saturate with decreasing temperature below T_c. At 35 meV the intensity peaks at ≈ 70 K as observed in $YBa_2Cu_3O_{6.85}$ [14], hinting at a nontrivial temperature dependence, which needs to be investigated further. Along L the upper branch has a broad maximum at $L = 1.7$; thus it is odd in the bilayer as is the resonance peak [Fig. 2(g)].

We then utilized the high resolution condition to focus on the two branches where they converge to 41 meV and $\mathbf{q}_{\rm AF}$. The constant **q** scan through $\mathbf{q}_{\rm AF}$ [Fig. 2(d)] shows the resonance peak at 41 meV, but the scattering has considerable broadening in **q** space at energies away from 41 meV [Fig. 2(b)]. However, the **q**-integrated $S(\mathbf{q}, \omega)$, $S(\omega)$, is roughly the same at all energies in Fig. 2(b) because of the broadening of $S(\mathbf{q}, \omega)$ along both H and K.

To get a more quantitative estimate of $S(\omega)$ we modeled the data (Fig. 2) with the following dispersions [solid lines in Fig. 3(c)]. For

$$33\ \text{meV} < \omega < \omega_0, \qquad \omega = -a|\mathbf{q} - \mathbf{q}_{\rm AF}|^2 + \omega_0,$$

and for

$$\omega > \omega_0, \qquad \omega = b|\mathbf{q} - \mathbf{q}_{\rm AF}|^2 + \omega_0,$$

where $\omega_0 = 41.2$ meV, $a = 191$ meV Å^2, and $b = 75$ meV Å^2 (values of b up to ≈ 100 give a good fit as

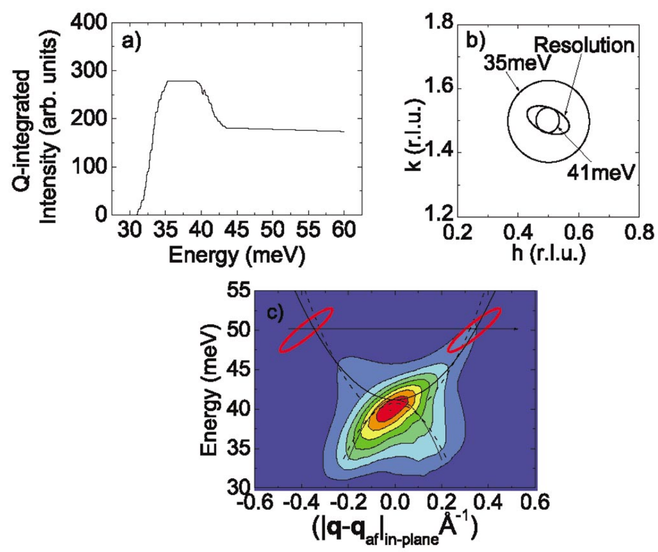

FIG. 3 (color). A model for $S(\mathbf{q}, \omega)$ in good agreement with most of the data (Fig. 2): (a) **q**-integrated density of states derived from the model. (b) Schematic of resolution effects in the a-b plane. The oval represents the a-b plane projection of the resolution ellipsoid, and the circles represent cuts of $S(\mathbf{q}, \omega)$ at $\omega = 40.5$ and 35 meV. Enhanced intensity at the resonance peak energy results from the entire $S(\mathbf{q}, \omega)$ fitting into the resolution ellipsoid near 41 meV. (c) Solid lines represent the **q**-ω dispersion relation. The color plot represents this model convoluted with experimental resolution. The tilt of resolution ellipsoid (red lines) results in better peak definition on the left and right sides for the upper and lower branches, respectively. The dashed line corresponds to a different dispersion that also fits the data.

well). The low-energy cutoff at 33 meV is the experimentally determined spin gap. An infinitely sharp (δ function of the above dispersions) $S(\mathbf{q}, \omega)$ gives a reasonably good agreement with the data (red lines in Fig. 2) in the lower branch, but is too narrow for the upper one. To better fit the data, a finite correlation length of 55 Å was included as well as an energy width of 2.2 meV FWHM (blue lines in Fig. 2). The upper to lower branch amplitude ratio of 0.65 best agrees with the data.

Experimental uncertainty allows slightly different values of ω_0, a, and b. A gap of <1 meV may exist between the branches or one or both branches may not "close" at $\mathbf{q}_{AF}$ [dashed line in Fig. 3(c)].

Fitting the scattering intensity at different energy transfers with the same amplitude places stringent constraints on the dispersion relation exponent. Powers higher than 2 would flatten the dispersion manifold near ω_0 and strongly enhance the predicted scattering intensity there, whereas powers lower than 2 would suppress it relative to the expectations of quadratic dispersion. Neither such enhancement or suppression is observed experimentally, which means that the quadratic terms dominate the dispersion relation. This also implies flat $S(\omega)$ in each branch [Fig. 3(a)]. The important caveat is that the differences between the data and the model at 51 and 55 meV hint at a more complex behavior there. Convergence of $S(\mathbf{q}, \omega)$ to $\mathbf{q}_{AF}$ at E_r [Fig. 3(b)] can account for all intensity in the resonance peak (Refs. [1,3]) as demonstrated by the excellent agreement between the model and the data in Fig. 2(d).

Somewhat similar $\mathbf{q}$-ω dispersions were reported for $YBa_2Cu_3O_{6.7}$ [13] and more recently for the stripe phase of $La_{1.875}Ba_{0.125}CuO_4$ [20]. They, however, exhibit a different temperature dependence as their observations are not limited to the superconducting state.

A number of theories predict or assume dispersive magnetic branches in copper oxide superconductors. A 2D metal with strong antiferromagnetic correlations in the d-wave SC state is characterized by dispersive magnetic collective modes [21]. The phenomenological spin-fermion model assumes an upward-dispersing branch though it does not predict the downward-dispersing one [22]. RPA calculations predict an incommensurate-commensurate-incommensurate magnetic signal evolution with energy [23,24]. Recent calculations based on the t-t'-J model [25] or going beyond the standard RPA [26] yielded results somewhat similar to ours. A quantitative comparison is required to further evaluate these models. Most importantly, many theories have to be reexamined in light of the finding that most spectral weight of magnetic excitations appears at energies above and below the resonance peak even at optimum doping.

The crystal growth was supported by the New Energy and Industrial Technology Development Organization (NEDO) as Collaborative Research and Development of Fundamental Technologies for Superconductivity Applications.

*To whom correspondence should be addressed.
Email address: reznik@llb.saclay.cea.fr

[1] J. Rossat-Mignod *et al.*, Physica (Amsterdam) **185–189C**, 86 (1991).
[2] H. A. Mook *et al.*, Phys. Rev. Lett. **70**, 3490 (1993).
[3] H. F. Fong *et al.*, Phys. Rev. Lett. **75**, 316 (1995).
[4] P. Bourges *et al.*, Phys. Rev. B **53**, 876 (1996).
[5] H. F. He *et al.*, Science **295**, 1045 (2002).
[6] H. F. Fong *et al.*, Nature (London) **398**, 588 (1999).
[7] P. Dai *et al.*, Phys. Rev. B **63**, 054525 (2001).
[8] Ar Abanov *et al.*, Phys. Rev. Lett. **89**, 177002 (2002), and references therein.
[9] M. Eschrig and M. R. Norman, Phys. Rev. B **67**, 144503 (2003), and references therein.
[10] H.-Y. Kee *et al.*, Phys. Rev. Lett. **88**, 257002 (2002).
[11] H. A. Mook *et al.*, Nature (London) **395**, 582 (1998).
[12] H. F. Fong *et al.*, Phys. Rev. B **61**, 14 773 (2000).
[13] M. Arai *et al.*, Phys. Rev. Lett. **83**, 608 (1999).
[14] P. Bourges *et al.*, Science **288**, 1234 (2000).
[15] S-W. Cheong *et al.*, Phys. Rev. Lett. **67**, 1791 (1991).
[16] J. M. Tranquada *et al.*, Phys. Rev. B **54**, 7489 (1996).
[17] J. D. Jorgensen *et al.*, Phys. Rev. B **41**, 1863 (1990).
[18] P. Schweiss (private communication).
[19] P. Bourges *et al.*, Phys. Rev. Lett. **90**, 147202 (2003).
[20] J. M. Tranquada *et al.*, Nature (London) **429**, 534 (2004).
[21] F. Onufrieva and P. Pfeuty, Phys. Rev. B **65**, 054515 (2002).
[22] D. K. Morr and D. Pines, Phys. Rev. Lett. **81**, 1086 (1998).
[23] M. R. Norman, Phys. Rev. B **63**, 092509 (2001).
[24] Y.-J. Kao *et al.*, Phys. Rev. B **61**, 11898 (2000).
[25] I. Sega *et al.*, Phys. Rev. B **68**, 054524 (2003); T. Tanamoto *et al.*, J. Phys. Soc. Jpn. **63**, 2739 (1994).
[26] I. Eremin *et al.*, Phys. Rev. B **69**, 094517 (2004).